ELSEVIER

Journal of Fluids and Structures 19 (2004) 349–368

JOURNAL OF FLUIDS AND STRUCTURES

www.elsevier.nl/locate/jnlabr/yjfls

A numerical study of flow-induced noise in a two-dimensional centrifugal pump. Part I. Hydrodynamics

M.A. Langthjem*, N. Olhoff

Institute of Mechanical Engineering, Aalborg University, Pontoppidanstræde 101, DK-9220 Aalborg East, Denmark

Received 23 December 2003; accepted 12 January 2004

Abstract

This paper is concerned with the simulation of the flow in a flat, 'two-dimensional' laboratory centrifugal pump. The main concern of the study is the calculation of the flow-induced noise. The aim of the present paper is to develop a computationally simple and fast method which is capable of giving a useful estimate of the noise-generating 'background-flow'. A companion paper describes the hydroacoustic part of the analysis. In the numerical flow model of the pump, the inlet is modelled by a point source and the blades of the impeller are covered with vortex elements with discrete, bound vortices. The casing is covered with source panels. Vortices are shed from the trailing edges of the impeller blades and convected with the streaming fluid in order to satisfy Kelvin's theorem. After computation of the velocity field, the fluid forces acting on the impeller blades are calculated by application of the unsteady Bernoulli equation. Some case studies of pump flows are presented. The acoustic properties of these flows is the subject of the second part of the paper.

1. Introduction

Noise generation within centrifugal pumps is receiving increasing research attention in recent years. This is due to increasingly strict environmental noise level restrictions, and also due to customer demands. In the past, the attention and research funding of 'machine acoustics' was mainly focused on high-speed noise, with application to aircraft and heavy-duty turbomachinery (Cumpsty, 1977). A few investigations have been concerned with analysis and minimization of the noise generation by low-speed fans and blowers (Neise, 1976; Jeon and Lee, 1999, 2000). As to centrifugal pumps, noise due to cavitation has received a good deal of attention through more than half a century (Stepanoff, 1957; Brennen, 1994). Research on noise generation not related to cavitation has been reviewed by Guelich and Bolleter (1992) and by Rzentkowski (1996). In recent years much work has been done on developing 'global' models, which are able to characterize the hydrodynamic sources from measured data (Mongeau et al., 1995; Morgenroth and Weaver, 1996; Rzentkowski and Zbroja, 2000). But it appears from the reviews that very little work has been done so far on mathematical models that include the influence of volute (casing) geometry on the acoustic pressure pulsations.

The present (two-part) paper attempts to follow a recommendation of Rzentkowski (1996) by suggesting a numerical procedure which ties the pump geometry with the noise sources. The present Part I of the paper will, as the title

*Corresponding author. Present address: Department of Mechanical Systems Engineering, Faculty of Engineering, Yamagata University, 4-3-16 Jonan, Yonezawa, Yamagata 992-8510, Japan. Tel.: +81-238-26-3326; fax: +81-238-26-3205.

E-mail address: mikael@yz.yamagata-u.ac.jp (M.A. Langthjem).

0889-9746/$ - see front matter
doi:10.1016/j.jfluidstructs.2004.01.003

Nomenclature

Roman symbols

a	chord (in airfoil example)
c_0	speed of sound
$\mathscr{C}_j$	cut-off function, defined by (4)
l_n	length of impeller blade panel n
$\mathscr{L}$	lift
M	Mach number
$\mathbf{n}$	normal vector
$N_{\ldots}$	number of …
p	fluid pressure
r	distance between source point $\mathbf{y}$ and observation point $\mathbf{x}$
r_T	impeller inner radius
R_T	impeller outer radius
s	curvilinear coordinate
t	time
t_{blade}	blade passage time, $2\pi/\Omega N_{\text{blades}}$
$\mathbf{t}$	tangential vector
U_T	rotor peripheral velocity, $R_T\Omega$
$\mathbf{x}$	observation point
$\mathbf{y}$	source point

Greek symbols

α	inclination angle (in airfoil example)
Γ	vortex/source strength
ε	cut-off radius in the function defined by (4)
ν	kinematic viscosity
ρ_0	fluid density
Ω	angular velocity

Subscripts

bi	bisector
bv	bound vortex
l	lower
ps	point source
sp	source panel
sv	shed vortex
t	tangent
u	upper
v	vortex

indicates, be concerned with the hydrodynamic part of the analysis. Part II (Langthjem and Olhoff, 2004) will be concerned with the hydroacoustic part.

As a 'first step' the analysis is restricted to a two-dimensional (2-D) formulation. A nearly 2-D flow field can be obtained in 'flat' laboratory pumps. In most commercial pumps, three-dimensional (3-D) effects cannot be neglected. But a 2-D analysis is much less computational demanding than a 3-D analysis and still, much essential understanding of the noise generation can be obtained.

The paper follows the 'acoustic analogy' point-of-view (Lighthill, 1952) where the analysis is separated into two steps. The first step is concerned with a hydrodynamic (incompressible) analysis, in order to obtain the 'background flow' and the noise-generating fluid forces. The second step is a hydroacoustic (compressible) analysis, which considers the solution of an inhomogeneous wave equation where the from 'step one' obtained fluid forces enter in the forcing function which drives the sound waves. This approach is valid when the acoustic back-reaction on the hydrodynamic field can be neglected. This is typically so when (i) the characteristic Mach number $M \ll 1$; (ii) compressibility is unimportant in determining the flow; (iii) the fluid motion is not coupled to a resonating system (Howe, 1997). For the

present centrifugal pump problem the appropriate Mach number is

$$M = \frac{\text{Impeller peripheral velocity}}{\text{Speed of sound}}, \tag{1}$$

and this is much less than unity for typical pumps. Pump systems also normally satisfy conditions (ii) and (iii).

The relation between unsteady flow, pressure fluctuations, and noise in centrifugal pumps has been studied experimentally by Chu et al. (1995) and by Dong et al. (1997). These papers give an excellent guideline to what is important to include in a mathematical model of the flow-induced noise. In Chu et al. (1995), the pressure inside the volute is calculated directly from the Reynolds equation by using phase-averaged velocities obtained from particle displacement velocimetry. Viscous stresses are ignored due to a high value of Reynolds number. The experiments are carried out using a pump with a '2-D' volute, and 2-D calculations compare well with measured pressure data. It is found that turbulence can be ignored, but vorticity gives a major contribution to the total pressure variation. A pure potential flow model (without shedding of vorticity) thus cannot provide an acceptable description of the flow. Another major conclusion is that the fluid–structure interaction between the rotating blades and the volute tongue may be the *primary source of noise generation*. This aspect was studied further by Dong et al. (1997). It was found by experiment that the noise level can be significantly reduced by increasing the gap between the tongue and the impeller up to about 20% of the impeller radius. [A standard pump has typically a gap of 5–10%.] But increasing the gap may decrease the pump hydraulic efficiency which is highly undesirable.

The interaction between the fluid, the rotating blades, and the volute tongue, and also the interaction between the flow and the rotating impeller alone, causes pressure fluctuations on the internal surfaces (stationary and moving) which acoustically correspond to *dipole sources*. Noise sources corresponding to monopole and quadrupole sources also exist in the pump, but it will be argued in Section 1 of Part II that these typically are insignificant in comparison to the dipole sources. It is thus assumed in this work that the noise generation within the pump is due to dipole sources alone. The reader is again referred to Part II for a discussion of this and other acoustics aspects.

There are many examples in the aeroacoustics literature where simple flow field estimates as input to an acoustic analogy-type of equation produce good estimates of both near- and far-field noise levels [see Howe (1998) for an extensive review; other interesting examples include Sugimoto and Ogawa (1998) and Jeon and Lee (1999)]. Encouraged by these examples, the idea starting the work to be presented here was to develop, within a 2-D framework, (i) a simple numerical method to compute a useful estimate of the oscillating fluid forces acting on the internal surfaces in a centrifugal pump and (ii) a method to compute the acoustic pressure fluctuations generated by these forces.

Considering task (i), it appears that the *discrete vortex method*, combined with the *panel method* for the solid surfaces, include those 'background flow' effects pointed out by Chu et al. (1995) as being important, and exclude those which are not. The discrete vortex method was introduced by Rosenhead (1931) in a study of vortex roll-up in the Kelvin–Helmholtz instability [see e.g., Drazin and Reid, 1981]. Recent reviews of vortex methods have been given by Graham (1986), Sarpkaya (1988) and Cottet and Koumoutsakos (2000), while panel methods are reviewed by Katz and Plotkin (2001). The discrete vortex method is an instationary, Lagrangian, grid-free method, useful to simulate flows with rotating mechanical components, as in a centrifugal pump. It was originally formulated for basically inviscid, high Reynolds number flows, with viscous effects entering only through the Kutta condition, to model the shedding of vorticity from surfaces into wakes. Once released, the vortices thus keep their initial strength throughout the simulation. In reality the vortex structures eventually die out due to viscous dissipation. To model this in a simple way, Kuwahara and Takami (1973) introduced 'artificial' viscosity, based on the exact solution of the equations of motion for a *single* vortex in an unbounded viscous fluid. Later, methods that deal rigorously with viscosity were developed [see Cottet and Koumoutsakos, 2000].

The 'inviscid' discrete vortex method with 'artificial' viscosity is chosen here, mainly due to its simplicity. But as the present work assumes a high Reynolds number flow, as is typical for many centrifugal pumps, the simple treatment of viscosity is believed to acceptable. The blades of the impeller are covered with vortex elements with discrete, bound vortices. The casing is covered with source panels (with continuous distributions of sources). During the simulation, discrete vortices are shed from the trailing edges of the impeller blades and the volute tongue. These vortices are convected with the streaming fluid, to form wakes.

Once the velocity field is known, the unsteady fluid forces acting on the impeller blades can be calculated by application of the (unsteady) Bernoulli equation. The fluid forces acting on the pump casing are evaluated in connection with the acoustic analysis, by making use of the boundary element method (see Part II).

The present paper is organized as follows. The mathematical flow model is described in Section 2. Section 2.1 describes the discrete vortex method and Section 2.2 the evaluation of the fluctuating blade forces. Section 3 describes verifications of individual components of the numerical scheme by comparisons with relatively simple problems

described in the literature. Section 4 is concerned with a numerical simulation of a pump described in Chu et al. (1995). Finally, some concluding remarks are made in Section 5.

2. Description of the mathematical flow model

2.1. The velocity field

A '2-D' laboratory pump will be considered, with a geometry as sketched in Fig. 1(a). The mathematical model is sketched in Fig. 1(b). [A very rough model is shown here, to emphasize the nature of the discretization. The actual computational model is shown in Fig. 5.]

The inlet is represented by a point source. This gives a 'perfect' inflow which is not found in an actual pump. Fluctuating inflow works acoustically as a monopole, which is the most efficient source type. Angular velocity variations may amplify a nonuniform outflow from the impeller, which also acts acoustically as a monopole. This could be modelled by placing several point sources of different strengths close to each other. Swirl could be modelled by point vortices. Such effects are however difficult to quantify, and the present study will only consider the perfect inflow from a single point source. Let $\mathbf{x} = (x_1, x_2)$ and $\mathbf{y} = (y_1, y_2)$ be points in the coordinate system $\mathbf{X} = (X_1, X_2)$, where $\mathbf{x}$ refers to an observation point, and $\mathbf{y}$ to the location of a singularity (sink, source, or vortex). If the source is located at $\mathbf{y}_{ps}$, the induced velocity at the position $\mathbf{x}$ is given by

$$\mathbf{u}_{ps}(\mathbf{x}) = \frac{\Gamma_{ps}}{2\pi} \frac{\mathbf{x} - \mathbf{y}_{ps}}{|\mathbf{x} - \mathbf{y}_{ps}|^2}, \tag{2}$$

where Γ_{ps} is the source strength.

The impeller blades are assumed to be very thin, such that they can be modelled as vortex sheets (or velocity discontinuities). These sheets are represented by vortex panels having discrete, bound vortices. In these 'lumped vortex' panels the vortices are placed at the panel quarter chord points, and control (or 'collocation') points are placed at the panel three-quarter chord points; see Fig. 2. These elements implicitly satisfy the Kutta condition at the trailing edge (Katz and Plotkin, 2001, p. 223). It is known that the flow often separates on the suction side before (upstream from) the trailing edge (Brennen, 1994, p. 41). This effect is ignored in the present model. Katz and Plotkin (2001, pp. 513–514) describe how separation from unknown locations may be included in the discrete vortex method. The method involves separation of many vortices from each blade at each time step, and thus becomes very computationally demanding in comparison with the present approach.

As already mentioned, vortices are shed from the trailing edges of the impeller blades and convected with the streaming fluid in order satisfy Kelvin's theorem (see the discussion to Eq. (9), below). The vortices used are so-called mollified versions (Cottet and Koumoutsakos, 2000) where the singularity at the vortex center is removed by multiplication with a smoothing 'cut-off function'. This is in order to avoid divergence of the numerical solution when two vortices get very close to each other. The induced velocity at $\mathbf{x}$ from a number of discrete vortices of strengths $(\Gamma_v)_j$

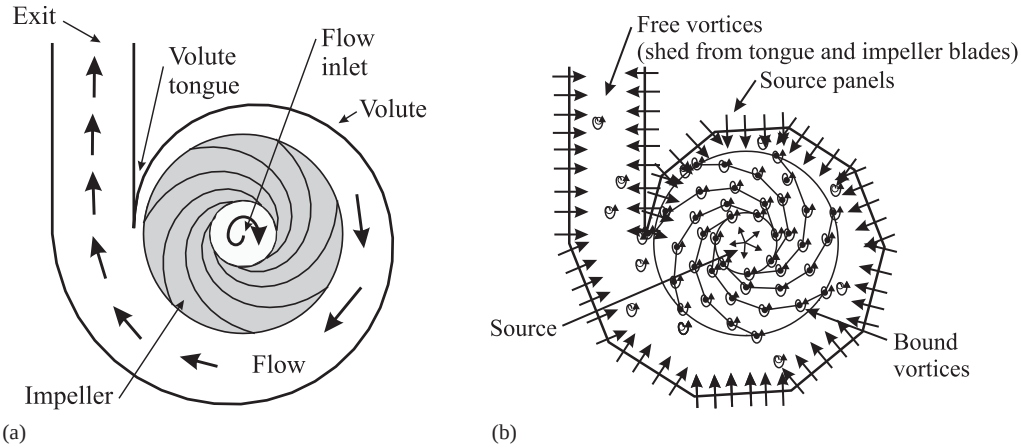

Fig. 1. (a) Schematic of a volute-type centrifugal pump; (b) Computational model (shown for a very rough discretization to emphasize the straight source panels).

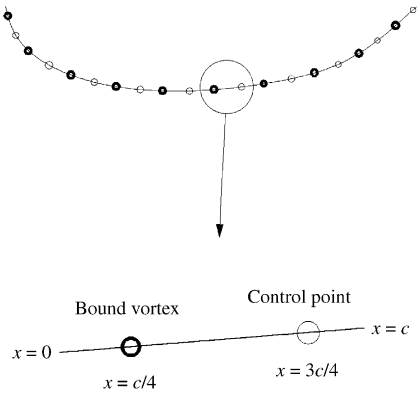

Fig. 2. Upper part: sketch of a single impeller blade covered with lumped vortex elements; Lower part: close-up of a lumped vortex element. The discrete, bound vortex is placed at the panel quarter chord point $x = c/4$; the control point is at the panel three-quarter chord point $x = 3c/4$.

located at $\mathbf{y}_j$, $j = 1, 2, \ldots, N_v$, is given by

$$\mathbf{u}_v(\mathbf{x}) = \sum_{j=1}^{N_v} \frac{(\Gamma_v)_j}{2\pi} \frac{(-x_2 + y_{2j}, x_1 - y_{1j})}{|\mathbf{x} - \mathbf{y}_j|^2} \mathscr{C}_j, \tag{3}$$

where $\mathscr{C}_j$ is the cut-off function given by

$$\mathscr{C}_j = [1 - \exp(-r_j^2/2\varepsilon^2)][1 + 2\exp(-r_j^2/2\varepsilon^2)], \quad r_j = |\mathbf{x} - \mathbf{y}_j| \tag{4}$$

and ε is the cut-off radius. Outside this (i.e. for $r > \varepsilon$) the velocity field is basically unaffected. With the induced velocity defined as in (3), a (single) vortex with a positive value of Γ_v will induce a counter-clockwise rotating flow.

The volute (pump casing) is covered by source panels, with uniform source strength over each panel. The induced velocity at $\mathbf{x}$ from N_{sp} source panels of constant strengths per unit length $(\Gamma_{sp})_j$ is written as

$$\mathbf{u}_{sp}(\mathbf{x}) = \sum_{j=1}^{N_{sp}} \frac{(\Gamma_{sp})_j}{2\pi} \mathbf{s}_j. \tag{5}$$

The influence coefficient vector $\mathbf{s}_j$ is derived in Appendix A. The volute is specified by N_{con} control points $\mathbf{p}_i = \{p_{1i}, p_{2i}\}$ which are interpolated by a B-spline curve, see e.g. Böhm et al. (1984). This kind of curve is defined by an expression on the form

$$\mathbf{r}(\xi) = (r_1(\xi), r_2(\xi)) = \sum_{i=0}^{N_{\text{con}}-1} \mathbf{p}_i B_i(\xi), \tag{6}$$

where ξ is a parameter and $B_i(\xi)$ are the B-spline basic functions. This parameterization of the volute curve has the advantage that, for equidistant values of the parameter ξ, the 'nodal points' $\mathbf{r}(\xi)$ are concentrated at sections with large gradients. Thus, by connecting the volute source panels to these nodal points, sections with large gradients will 'automatically' be covered by many small panels, while relatively straight sections will be covered with fewer, larger panels.

The total induced velocity at $\mathbf{x}$ is given by

$$\mathbf{u}(\mathbf{x}) = \mathbf{u}_{ps}(\mathbf{x}) + \mathbf{u}_{sp}(\mathbf{x}) + \mathbf{u}_{bv}(\mathbf{x}) + \mathbf{u}_{sv}(\mathbf{x}), \tag{7}$$

where index bv denotes bound vortices and index sv shed vortices. The boundary conditions are given by

$$\mathbf{u}(\mathbf{x}_k) \cdot \mathbf{n}_k = \begin{cases} \Omega \mathbf{r}_k \cdot \mathbf{n}_k & \text{on impeller blade panel number } k, \\ 0 & \text{on the pump casing,} \end{cases} \quad k = 1, 2, \ldots, N_{cp}, \tag{8}$$

where N_{cp} is the total number of control points, $\mathbf{r}_k$ is the radius-vector to impeller blade control point k, $\mathbf{n}_k$ is the normal vector, and Ω is the angular velocity. The strength Γ_{new} of the new vortex to be shed from the trailing edge of impeller

blade j is calculated by using Kelvin's theorem, which says that: "The circulation around a closed curve moving with the fluid remains constant" (Lighthill, 1986). As the circulation is zero at start-up of the pump, the sum of all vortex strengths must remain zero at any time, giving

$$\left[\sum_{m=1}^{N_{bv}} (\Gamma_v)_{mj} + \sum_{n=1}^{N_{\text{shed}}} (\Gamma_{sv})_{nj} + (\Gamma_{\text{new}})_j\right]_j = 0, \quad j = 1, \ldots, N_{\text{blades}}, \tag{9}$$

where N_{shed} is the number of vortices shed from blade number j. The vortices are released at a small distance ϵ from the edges, at positions $\epsilon \mathbf{t}_j^{\text{edge}}$, where $\mathbf{t}_j^{\text{edge}}$ is the tangent vector.

Vortices are also shed from the tip of the volute tongue. The strengths of these vortices are determined by imposing the Kutta condition at the tip, although this is a leading edge, rather than a trailing edge. [See Crighton (1981, 1985) for critical reviews of the concept of applying the Kutta condition to unsteady leading edge flows.] Mathematically the condition is expressed as

$$\mathbf{u}(\mathbf{x}_{\text{tip}}) \cdot \mathbf{n}_{bi} = 0, \tag{10}$$

where $\mathbf{x}_{\text{tip}}$ is the tip point and $\mathbf{n}_{bi}$ is the normal to the bisector of the tongue's edge angle. Some blunt (rounded) volute tongues will also be considered in Part II, in addition to sharp ones. Although the stagnation point for such tongues are not fixed [see Dong et al., 1997] it will, for simplicity, be assumed fixed at the point of maximum curvature.

Eqs. (8)–(10) constitute together $N = (N_{bv} + 1)N_{\text{blades}} + N_{sp} + 1$ linear equations with N unknown vortex strengths $\mathbf{\Gamma} = (\Gamma_1, \Gamma_2, \ldots, \Gamma_N)^{\text{T}}$. After each time increment Δt the impeller coordinates and positions of shed vortices are updated and the equation system is resolved. Once the vector $\mathbf{\Gamma}$ is determined, the flow velocity can be evaluated at any point. The position of each of the shed vortices is updated according to the second-order scheme (Kiya et al., 1982)

$$\mathbf{x}_{sv}(t + \Delta t) = \mathbf{x}_{sv}(t) + \tfrac{1}{2}\{3\mathbf{u}(\mathbf{x}_{sv})_t - \mathbf{u}(\mathbf{x}_{sv})_{t-\Delta t}\}\Delta t. \tag{11}$$

Vortices that have left the exit of the pump are ignored in the following time steps. New vortices are released at every second time increment, i.e.

$$\Delta t_{\text{release}} = 2\Delta t, \tag{12}$$

as suggested by Sarpkaya and Ihrig (1986).

Following Kiya et al. (1982), the strength of every free vortex is reduced according to

$$\Gamma(t) = \Gamma_0\left\{1 - \exp\left(\frac{-r_c^2}{4\nu t_\omega}\right)\right\}, \tag{13}$$

such as to include viscous dissipation in a simple way. It has been found necessary to do this to damp out the unphysical, 'sharp' velocity fluctuations that otherwise will be generated when the pump is filled with vortices. [The model is similar to the Lamb–Oseen vortex model, see Sarpkaya, 1988.] $t_\omega = t - t_{\text{release}}$ is the age of the vortex, Γ_0 is its initial strength, and ν is the kinematic viscosity of the fluid. r_c is a fixed radius which magnitude most authors base on numerical experimentation, in order to obtain the closest agreement between calculation and experiment (Kiya et al., 1982; Graham, 1986). In the present work,

$$r_c = g_{\min}/20 \tag{14}$$

was used, where $g_{\min}$ is the smallest gap between impeller and volute tongue. [A more rigoristic approach to the choice of r_c would clearly be desirable, but it is beyond the scope of the present paper to go further into this problem.]

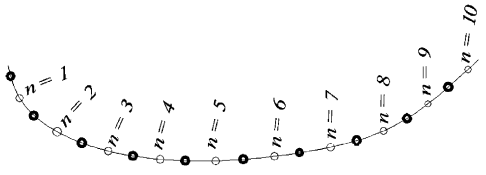

Fig. 3. Illustration of the control point enumeration used in Eqs. (15) and (16). The numbering continues on the next blade; the numbers are here $n = 11$ through 20, and so on through all blades.

2.2. Fluctuating surface pressure

When the velocity field has been computed, the unsteady fluid forces acting on the impeller blades can be evaluated by applying small velocity perturbations to the (unsteady) Bernoulli equation for a rotating system [e.g. Batchelor, 1967, p. 162]. The pressure a small distance ϵ above the control point of element n (see Fig. 3) is

$$(p_u)_n = p_0 + \tfrac{1}{2}\rho_0(u_t)_0^2 - \tfrac{1}{2}\rho_0(u_t + \Delta u_u)_n^2 - \tfrac{1}{2}\rho_0\Omega^2(r_0^2 - r_n^2)_u - \rho_0\int_{s_0}^{s_n}\frac{\partial}{\partial t}(u_t + \Delta u_u)\,\mathrm{d}s, \tag{15}$$

where s is a curvilinear coordinate, ρ_0 is the mean density of the fluid, u_t is the tangential velocity, Δu_u is a small increment thereto, and r is the radius (measured from the impeller axis). The point "0" is a little upstream of the impeller blade. The expression for the pressure $(p_l)_n$ a small distance ϵ below the element takes the same form, just with index u replaced by index l. Using that $(\Delta u_u)_n - (\Delta u_l)_n = (\Gamma_v)_n/l_n$ (Katz and Plotkin, 2001, p. 73), and neglecting terms that are quadratic in the small disturbances Δu_u, Δu_l, the pressure difference $\Delta p_n = (p_l)_n - (p_u)_n$ can be written as

$$\Delta p_n \approx \rho_0 u_{tn}(\Gamma_{bv})_n/l_n + \rho_0\sum_{j=1}^{n}\frac{\partial(\Gamma_{bv})_j}{\partial t}, \tag{16}$$

where l_n is the length of impeller blade panel number n. The first term has the form of the Kutta–Joukowski theorem $L = \rho_0 U\Gamma$ for the lift L on a airfoil with circulation Γ and speed U.

The assumption of thin blades has been applied to obtain (16), such that the Coriolis force term $\frac{1}{2}\rho_0\Omega^2\{(r_n^2)_l - (r_n^2)_u\}$ can be ignored. Neglect of the terms quadratic in the disturbances Δu_u and Δu_l is, strictly speaking, permissible only if the angular speed $|r\Omega| \gg |\Delta u_u|, |\Delta u_l|$. Alternatively, $\Delta p_n = (p_l)_n - (p_u)_n$ could be evaluated directly by using (15) and the corresponding equation for $(p_l)_n$, taking the small distance ϵ as the half impeller thickness. But (16) is the appropriate expression for the pressure difference across blades of vanishingly small thickness, i.e., representation of the blades by vortex sheets, as used in the present work. It is noted here that velocity computations are 'expensive' as they, for any evaluation point, involve summation over all vortices. Direct computation of $\Delta p_n = (p_l)_n - (p_u)_n$ involves twice as many velocity evaluations as (16). It should also be noticed that in cases of large disturbances, where the sufficiency of the linearized form of the first term might be doubted, the second, unsteady term will dominate over the first, and no approximations have been made in this term.

The time derivative of the last term in (16) must be evaluated numerically. As 'jitter' in the velocities is unavoidable by the discrete vortex method, a direct finite difference approach will amplify the noise and yield results of limited value. A smoother and more useful pressure time series can be obtained by differentiating a least-square fit of a number of consecutive points on the 'Γ_{bv} curve', as suggested by Lanczos (1956).[1] The formula for the general case of smoothing by use of K neighbors on both sides of the point where the derivative is wanted is given by

$$\frac{\partial\Gamma(t)}{\partial t} = \left(\sum_{k=-K}^{K} k\Gamma(t + k\Delta t)\right) \Big/ \left(2\sum_{k=1}^{K} k^2\Delta t\right). \tag{17}$$

As values ahead are needed, the pressure evaluation must lag K time steps after the actual state. If $K = 2$, for example, the formula is

$$\frac{\partial\Gamma(t - 2\Delta t)}{\partial t} = \{-2\Gamma(t - 4\Delta t) - \Gamma(t - 3\Delta t) + \Gamma(t - \Delta t) + 2\Gamma(t)\}/10\Delta t. \tag{18}$$

In the present work, $K = 8$ was used.

2.3. Which noise sources does the flow model include?

Flow-noise sources[2] may be classified into (i) monopoles, corresponding to unsteady sources; (ii) dipoles, corresponding to unsteady surface pressure forces; (iii) quadrupoles, corresponding to turbulent velocity- and pressure-fluctuations. The monopole is the most efficient noise source; the quadrupole is the least efficient.

Nonuniform and unsteady outflow from the impeller, between two consecutive impeller blades, may act as monopole sources. And interaction between the shed vortices may emulate turbulent flow, acting as quadrupole sources.

[1] A slightly different approach, based on so-called 'smooth interpolatory subdivision algorithms' was recently suggested by Qu (1996). The formulas take the same form as Lanczos's, but the weighing coefficients are different.

[2] Please see Part II for a more detailed discussion.

The acoustic analysis of Part II will, however, only consider noise from dipole sources. The quadrupole sources are typically much weaker and furthermore very difficult to quantify correctly (Fedorchenko, 2000). The monopole sources are also typically much weaker in well-designed pumps. This is, admittedly, an important point to verify for the present model, but it will be postponed to a future study.

The present flow model includes dipole-type sources, related to pressure fluctuations on the surfaces, due to the interaction between the rotating impeller blades and (i) the volute tongue, (ii) the 'background flow', and (iii) the shed vortices; and (iv) interaction between the shed vortices and the volute tongue. All these effects contribute to the pressure pulsations. An example in Section 4.2 will illustrate the influence of the shedding of vortices on the pressure pulsations on the impeller blades. But it is difficult to assess the relative importance of the contributions (i)–(iv) on the noise generation, as leaving out the vortex shedding, for example, will result in an erroneous, 'unphysical' flow.

3. Verification of individual routines in the numerical method

As the flow in a centrifugal pump is very complex some relatively simple test problems with analytical solutions were considered, to validate the individual parts of the numerical method. The source panels modelling the casing were checked by reproducing the potential flow past a cylinder. The lumped vortex panels representing the casing were checked by considering a flat plate suddenly set into motion. The reason for choosing this problem is that it effectively validates the instationary pressure term in (16), and yet, it is a simple problem to program. Fig. 4(a) shows the thin flat plate with a chord length of $2a$, inclined $\alpha = 5^\circ$ with respect to the x-axis, after impulsive start-up to a constant speed U of rectilinear motion along the x-axis. The figure also shows the vortex roll-up. Fig. 4(b) shows the growth of circulation and lift. These quantities have been scaled with the asymptotic values (for $t \to \infty$) which are $\Gamma_\infty = 2a\pi U \sin\alpha$ and $\mathscr{L}_\infty = 2a\rho_0 U\Gamma_\infty$, respectively. It will be seen that there is very good agreement between the analytical results given by Katz and Plotkin (2001, p. 383) and the discrete vortex results.

4. Simulation of the flow in a centrifugal pump

4.1. Description of geometry

Computations are performed for the '2-D' laboratory pump of Chu et al. (1995). The pump speed is 890 r.p.m. The impeller is 253 mm in outer diameter and 84 mm in inner diameter. It has seven blades, all with an exit angle of 15° and formed as logarithmic spirals. The blades are made of thin plate of uniform thickness. The volute has the shape of a simple Archimedes spiral, with radius

$$r_v(\theta) = R_T + g_{\min} + g_v(\pi - \theta)/2\pi, \quad -\pi \leqslant \theta \leqslant \frac{59}{60}\pi. \tag{19}$$

Here $R_T = 126.4$ mm is the outer radius of the impeller, $g_{\min} = 9$ mm is the minimum volute gap, and $g_v = 102$ mm is the 'main' volute gap. Often the lip clearance is specified in per cent of the impeller radius. In this example, 100% ×

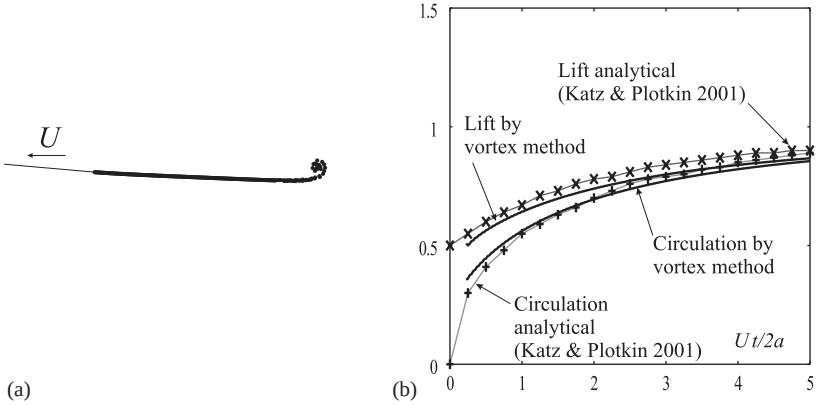

Fig. 4. (a) Roll-up of the vortex wake from a flat plate, inclined 5° to the axis of motion, which was started up impulsive from rest to the speed U; (b) Lift and circulation. Comparison between computational results and analytical results from Katz and Plotkin (2001).

$g_{\min}/R_T \approx 7\%$. A straight exit channel of height 4 m is connected to the pump at the volute end-points $\theta = -\pi$ and $\theta = \frac{59}{60}\pi$. The strength of the inlet source is 0.675 $m^2 s^{-1}$ (flow rate per unit depth). For a volute of constant thickness 25 mm, this gives a flux of 1.022 m^3/min which is 35% above the design flow rate, as also used in the tests of Chu et al. (1995). The working fluid is pure water with mean density $\rho_0 = 1000\ kg\,m^{-3}$ and speed of sound $c_0 = 1400\ m\,s^{-1}$. If the kinematic viscosity $\nu = 1.004 \times 10^{-6}\ m^2 s^{-1}$ (pure water at 20°C), the Reynolds number is $\mathrm{Re} = 2R_T U_T/\nu = 2\Omega R_T^2/\nu \approx 3 \times 10^6$ (Brennen, 1994). The largest rotational Mach number is $M_r = U_T/c_0 = \Omega R_T/c_0 \approx 0.0084$.

The technical data for the pump are summarized in Table 1. The computational parameters are given in Table 2.

4.2. Simulation results and discussion

Fig. 5 shows the distribution of the vortices shed from the tongue and the trailing edges of the impeller blades after impulsive start-up from rest to 890 r.p.m. of the seven-bladed centrifugal pump. The impeller rotates in clockwise direction and is moved 2° forward by each time-step. Black asterisks indicate anti-clockwise rotating vortices, while open dots indicate clockwise rotating ones. Vortex roll-up may be noticed in Figs. 5(a) and (b). This roll-up is in correspondence with the counter-clockwise rotation of fluid within each blade passage, which sometimes is called the displacement flow (Brennen, 1994).

Fig. 6(a) shows the distribution of vortices after 200 time-steps (corresponding to an impeller increment of 400°) from impulsive start-up from rest. Part (b) shows the corresponding velocity vectors, part (c) the iso-velocity levels, and part (d) the iso-vorticity levels. The recirculation seen on the outside of the volute tongue (especially clear from parts (b) and (c)) is here mainly due to the shedding of vortices from the volute tongue, but is amplified when the flow rate is above the design flow rate (Brennen, 1994). These plots appear to be consistent with Figs. 2 and 3 in Chu et al. (1995). The vorticity ξ_z in Fig. 6(d) was calculated by approximating $\xi_z = \partial u_2/\partial x_1 - \partial u_1/\partial x_2$ by the finite difference expression

Table 1
Data for the simulated centrifugal pump

Parameter	Symbol	Specification
Impeller inner radius	r_T	42.1 mm
Impeller outer radius	R_T	126.4 mm
Number of blades	N_{blades}	7
Blade exit angle	—	15°
Blade shape	—	Logarithmic spiral
Pump vane perimeter	r_v	$[R_T + 9 + 102(\pi - \theta)/2\pi]$ mm, $(-\pi \leqslant \theta \leqslant \frac{59}{60}\pi)$
Length of exit pipe	—	4 m
Flow rate	—	1.35 × design flow rate = 1.022 m^3/min
Design flow rate	—	0.757 m^3/min
Angular velocity	Ω	93.2 rad s^{-1} (890 r.p.m.)
Peripheral impeller velocity	U_T	11.78 m s^{-1}
Fluid density	ρ_0	1000 kg m^{-3}
Fluid kinematic viscosity	ν	$1.004 \times 10^{-6}\ m^2\ s^{-1}$
Speed of sound	c_0	1400 m s^{-1}

Table 2
Computational parameters

Parameter	Symbol	Specification
Number of panels on each impeller blade	N_{bv}	40
Number of panels on the pump casing	—	40
Number of panels on the exit pipe	—	80
Inlet source strength	Γ_{ps}	0.675 $m^2\ s^{-1}$
Vortex cut-off radius	ε	0.005 m

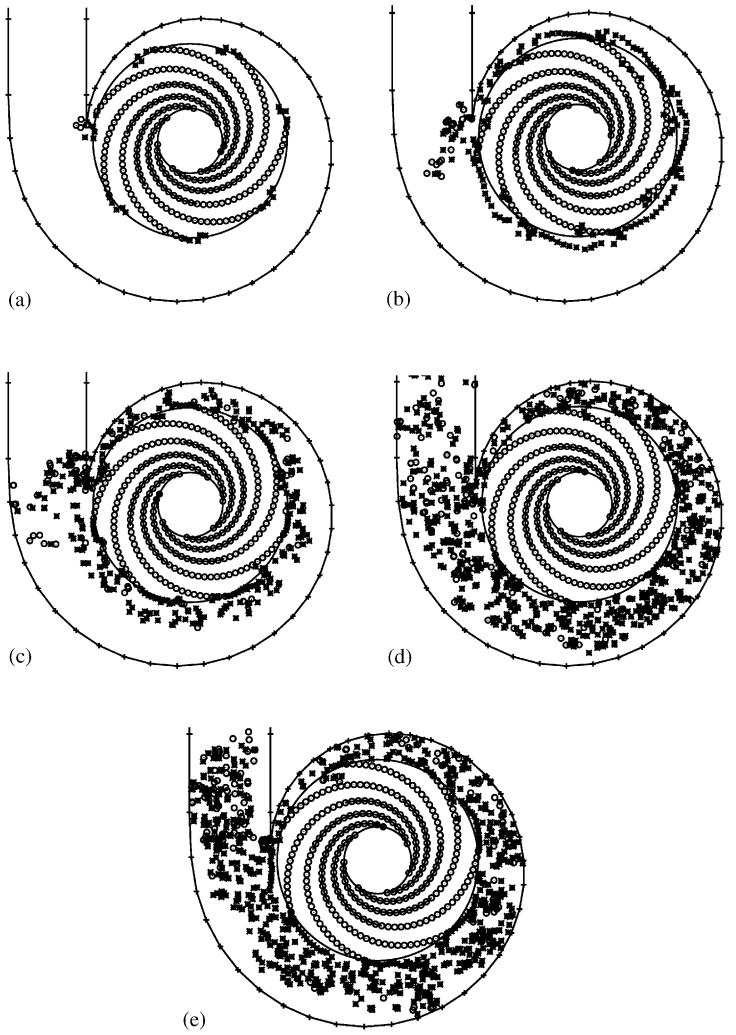

Fig. 5. Distribution of shed vortices after impulsive start-up of a pump from 0 to 890 r.p.m. Black asterisks indicate anti-clockwise rotating vortices, open dots indite clockwise rotating ones. The division of the volute into panels is also indicated. The number of time steps are: (a) 10; (b) 50; (c) 100; (d) 500; and (e) 5000. The impeller is advanced 2° at each time step.

$\xi_z = \Delta u_2/\Delta x_1 - \Delta u_1/\Delta x_2$. If the cut-off function $\mathscr{C}_j \equiv 1$ in (3) the vorticity field will just be given by

$$\xi_z = \begin{cases} (\Gamma_v)_j & \text{for } (x_1, x_2) = (y_{1j}, y_{2j}), \\ 0 & \text{for } (x_1, x_2) \neq (y_{1j}, y_{2j}), \end{cases} \tag{20}$$

where again, (x_1, x_2) is the observation point and $(\Gamma_v)_j$ is the strength of the vortex placed at (y_{1j}, y_{2j}). But with $\mathscr{C}_j$ given by (4) the vorticity will be nonzero away from the discrete vortices (Tryggvason et al., 1991).

Fig. 7(a) shows the variation in strength of the vortices shed from the impeller blades. Here $t_{\text{blade}} = 2\pi/\Omega N_{\text{blades}}$ is the time between the passing by the tongue of two consecutive impeller blades. Pulse-like spikes are thus seen at every seven time units, where a blade passes by the volute tongue. Fig. 7(b) shows the nondimensional lift and circulation for one impeller blade, defined by $\mathscr{L}_{\text{tot}} = \sum_n \Delta p_n/\rho_0 U_T^2$ and $\Gamma_{\text{tot}} = \sum_n (\Gamma_n/U_T l_n)$, respectively. A periodic pattern is recognized, but also some random 'noise' due to the interaction of vortices. With a nondimensionalization of the time t by $7t_{\text{blade}}$, one time unit corresponds to a full rotation of the impeller. Negative circulation corresponds to the

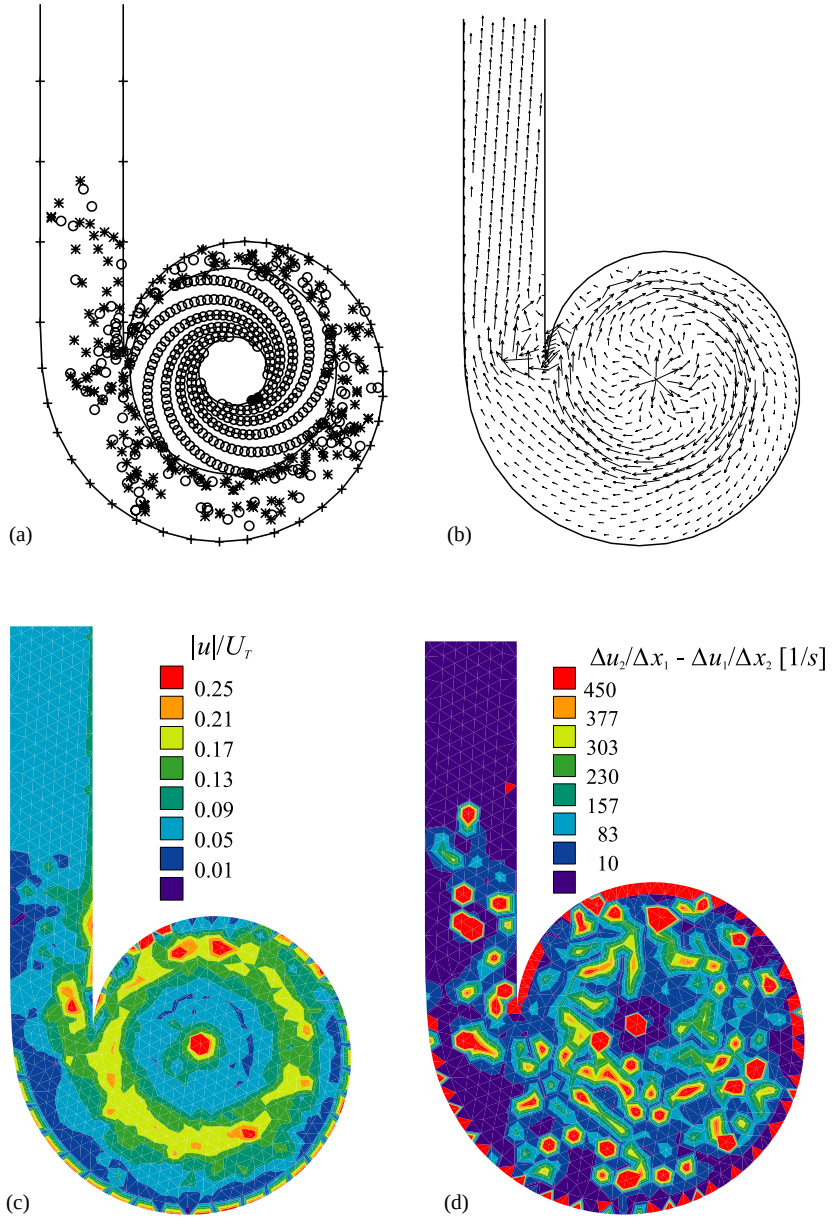

Fig. 6. (a) Distribution of vortices at 200 time-steps after impulsive start-up from rest. The impeller is advanced 2° at each time-step; (b) Velocity vectors; (c) Iso-velocity levels; (d) Iso-vorticity levels.

generation of counter-clockwise rotating eddies between the blades, and to lift in the convex direction. It is noted that the change of sign of the lift is made possible by the nonstationary (time-derivative) term in (16).

This is perhaps illustrated better by Fig. 8 (full lines) which shows (a) the nondimensional tangential velocity u_{tn}/U_T and (b) the pressure difference $\Delta p_n/\rho_0 U_T^2$ for the most downstream control point ($n = N_{bv}$) of an impeller blade. Guelich and Bolleter (1992) estimate the absolute velocity and the variation in stagnation pressure, caused by the wake flow, at an impeller outlet to be of magnitudes $u_t \approx 0.5 U_T$ and $\Delta p \approx 0.375 \rho_0 U_T^2$, respectively, but mention that values of $\Delta p/\rho_0 U_T^2$ between 0.4 and 0.5 have been measured. These values are seen to agree reasonably well with the results presented in Fig. 8. Having the Bernoulli equation in mind, it may seem strange that maximum stagnation pressure

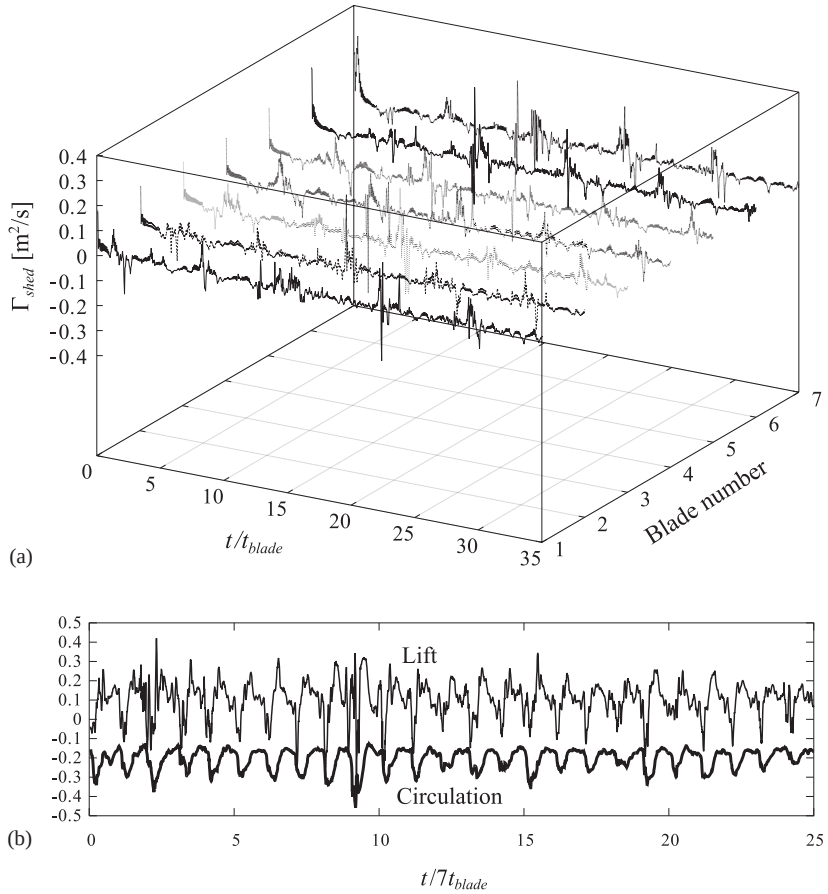

Fig. 7. (a) Variation in the strength of the vortices that are shed from the trailing edges of the impeller blades; (b) Variation in total lift and total circulation of a single impeller blade.

corresponds to maximum tangential velocity. This is because the tangential velocity is given with respect to global (fixed) coordinates, and not with respect to a coordinate system rotating with the impeller. In such a coordinate system, maximum stagnation pressure corresponds to minimum tangential velocity. [See also Fig. 2 in Guelich and Bolleter (1992) and the discussion thereto.] Fig. 8(b) also illustrates the importance of the unsteady term in (16). Without the unsteady term the pressure fluctuations are small, and the 'pulse' generated when the blade passes by the volute tongue is not captured at all.

The influence of vortex shedding on the tangential (absolute) velocity and the variation in stagnation pressure at the impeller outlets is also illustrated by Fig. 8 (dashed lines). Kelvin's theorem (Eq. (9)) is violated in the absence of vortex shedding, although the velocity boundary conditions are satisfied. The result is a significantly too low exit flow velocity, an unphysical velocity peak when the wake flow is blocked by the tongue (Fig. 8(a)), and thus also a very different pressure signature (Fig. 8(b)).

The effects of both spatial and temporal discretizations are illustrated in Figs. 9–12. These figures show, as Fig. 8, the variations in velocity and stagnation pressure at the most downstream control point of an impeller blade. In any of the figures, only one parameter is changed at a time. Fig. 9 shows the effect of dipole density on the impeller blades. [It should be noticed here that when the number of dipoles are changed the locations of the control points are also changed slightly.] Fig. 10 shows the effect of changing the time step, in terms of the impeller degrees of advancement per time step. Fig. 11 shows the effect of panel density on the volute, and Fig. 12 the effect of panel density on the exit pipe. Although differences are seen, it is difficult to trace any general trend in any case. It may then be concluded that results based on the computational parameters of Table 2 are sufficiently insensitive to discretization changes.

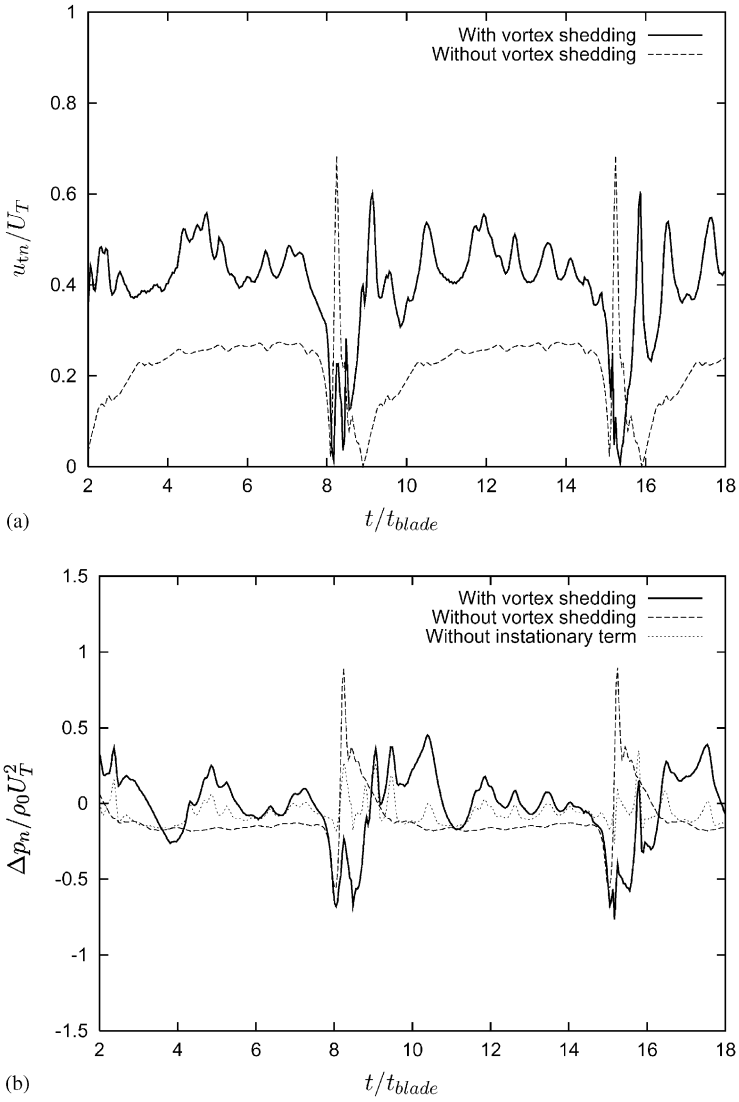

Fig. 8. Effect of vortex shedding from the impeller blades. (a) Variation in tangential velocity u_{tn}/U_T at the most downstream control point of an impeller blade; (b) Variation in pressure difference $\Delta p_n/\rho_0 U_T^2$ at the same location.

Following the pattern of Figs. 8–12, Fig. 13 illustrates the effect of changing the pump speed, while keeping the flow rate constant (in terms of constant inlet source strength). Reducing the speed from 890 to 800 r.p.m. does, as might be expected, not significantly influence the velocity and stagnation pressure. Reduction to 600 r.p.m. results in lower maximum velocity, and smoother velocity variations. This implies in turn a smoother variation in stagnation pressure. The pulse-like spikes on both velocity and pressure curves for 600 r.p.m. are caused by 'squeezing' of a vortex when an impeller blade passes by the volute tongue.

Fig. 14 illustrates the effect of changing the flow rate, in terms of the changing the inlet source strength. The speed is kept constant equal to 890 r.p.m.. Reducing the source strength results in more 'noise' in the velocity and pressure. This is because the shed vortices are then not so well 'shed clear' from each other, and noisy interactions occur. [The lowest flow rate, 0.5 $m^2 s^{-1}$, is, in fact, the design flow rate.] In spite of the increased noise, there is a tendency of more abrupt velocity and pressure changes, indicating larger pressure pulsations by decreased flow rate.

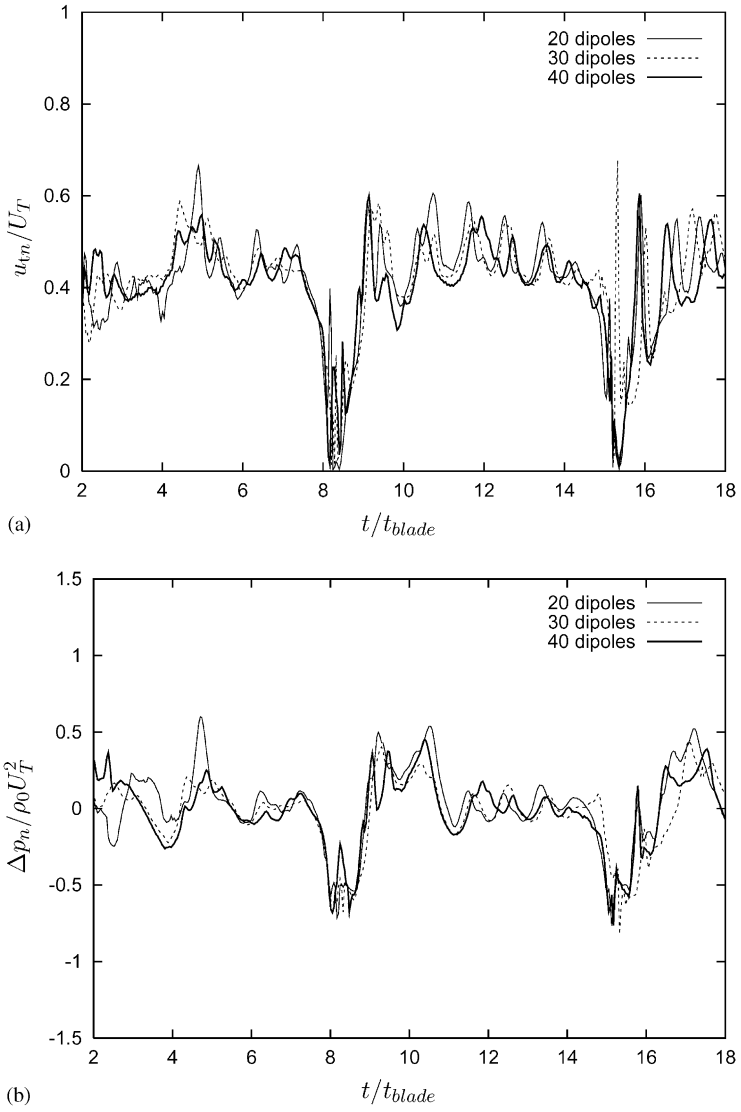

Fig. 9. Effect of dipole density on the impeller blades. (a) Variation in tangential velocity u_{tn}/U_T at the most downstream control point of an impeller blade; (b) Variation in pressure difference $\Delta p_n/\rho_0 U_T^2$ at the same location.

Returning, lastly, to the velocity and pressure fluctuations shown in Fig. 8, Fig. 15 shows the frequency spectra of these signals. It is seen that both fluctuate with the rotational frequency $f_{\text{rot}} = \Omega/2\pi = 14.8$ Hz and its higher harmonics. [It is noted that the second harmonic is the dominating frequency in the pressure signal.] This indicates that the responding pressure fluctuations in the volute will be dominated by the blade passage frequency $f_{\text{blade}} = f_{\text{rot}} N_{\text{blades}} = 103.8$ Hz and its higher harmonics, corresponding to the integrated effect of all N_{blades} impeller blades.

5. Conclusion

This paper has presented a discrete vortex method for simulation of the flow within a centrifugal pump. It is believed to be one of the simplest methods capable of capturing the essential features of this kind of rotational flow. The aim of

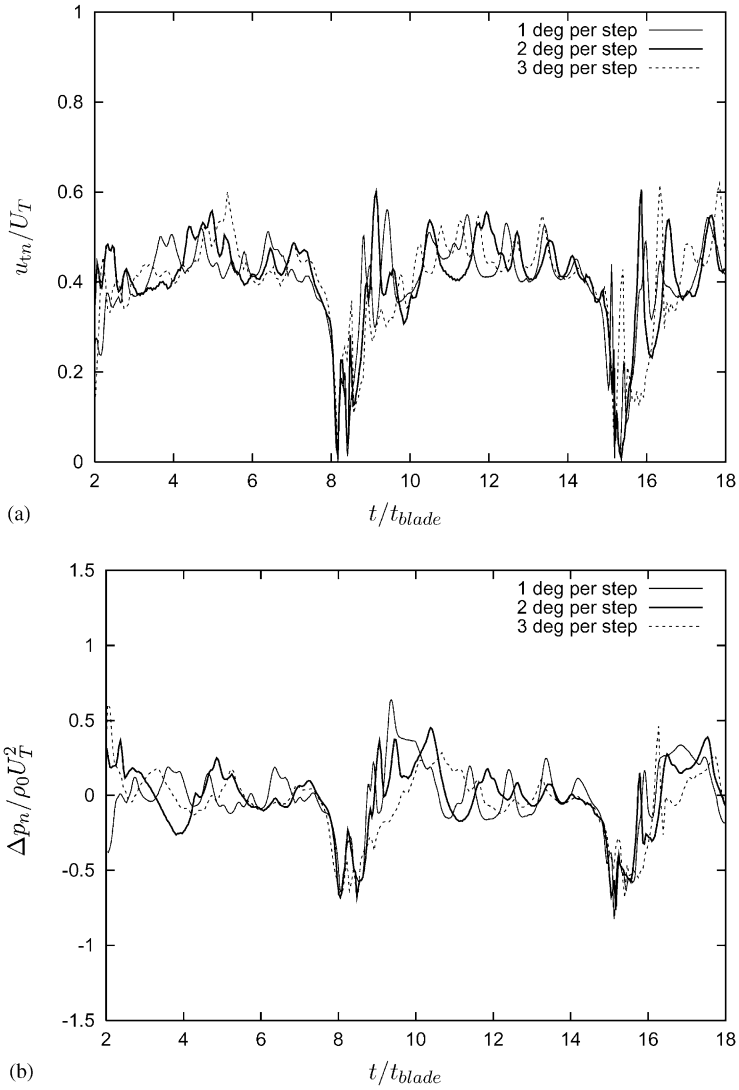

Fig. 10. Effect of the size of the time steps, in terms of number of degrees of impeller advancement per time step. (a) Variation in tangential velocity u_{tn}/U_T at the most downstream control point of an impeller blade; (b) Variation in pressure difference $\Delta p_n/\rho_0 U_T^2$ at the same location.

the method is, in the present context, to provide a good estimate of the unsteady impeller blade surface forces as input to an acoustic model, which is the subject of Part II of the paper.

The method is inherently 2-D. It is thus sufficient for analyzing the laboratory pump flow to which it has been applied, as experiments have shown that the flow indeed is essentially 2-D. 3-D effects can hardly be neglected in most commercial pumps, and the usefulness of the discrete vortex method to such complicated problems is uncertain, as 3-D vortex methods still are on an early stage of development (Satofuka, 2000).

The main conclusions from the examples presented are as follows.

(i) It is essential to take the shedding of wake vorticity into account in order to obtain realistic wake flow velocities.

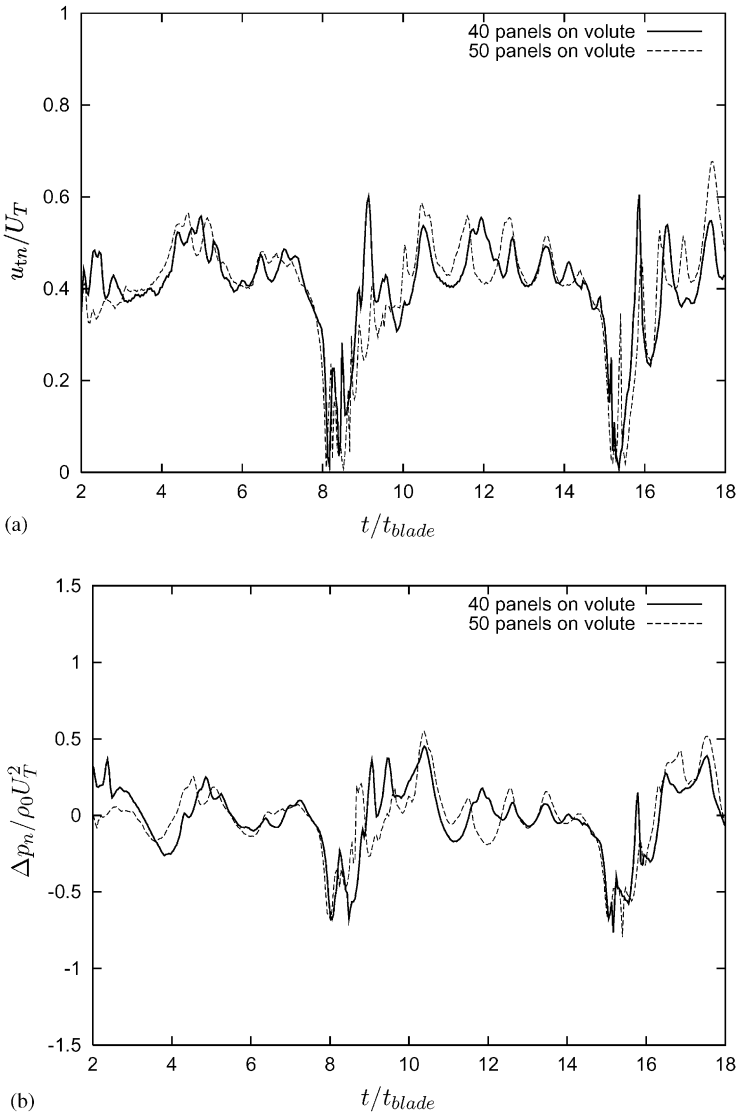

Fig. 11. Effect of panel density on the volute. [There are 80 panels on the exit channel in any case.] (a) Variation in tangential velocity u_m/U_T at the most downstream control point of an impeller blade; (b) Variation in pressure difference $\Delta p_n/\rho_0 U_T^2$ at the same location.

(ii) The velocity and pressure fluctuations on the impeller blades are dominated by the rotational frequency $f_{\text{rot}} = \Omega/2\pi$ and its higher harmonics.
(iii) Lanczos's (1956) method to determine the derivative of a time series has been found very useful.

Acknowledgements

Financial support from Aalborg University, Grundfos A/S, the Alexander von Humbolt Foundation, and the Danish Ministry of Research is gratefully acknowledged. We are most grateful for the helpful discussions with A. Back-Pedersen, K.S. Dahl, C.B. Jacobsen and J.B. Nielsen of Grundfos A/S. Helpful suggestions by Professor D.S. Weaver are gratefully acknowledged. We also wish to thank the referees for many helpful suggestions to improve the paper. The first author (M.L.) would finally like to thank Professors H. Umemiya and M. Nakano at Yamagata University for the opportunity to complete this work.

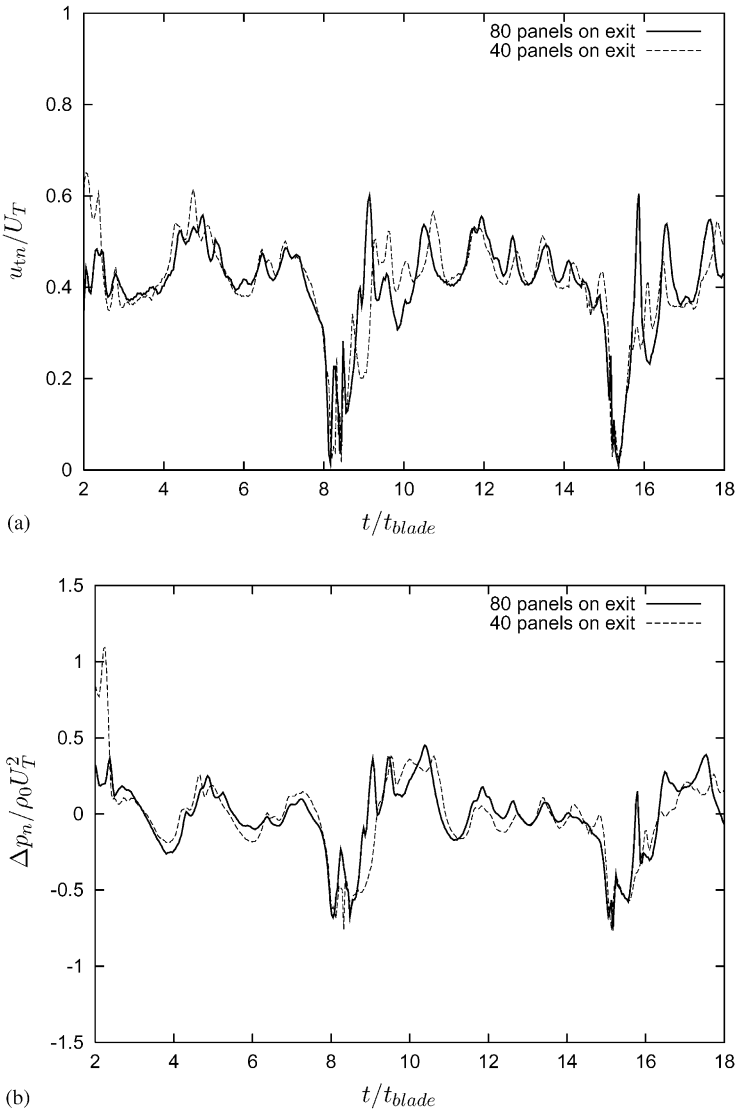

Fig. 12. Effect of panel density on the exit channel. [There are 40 panels on the volute in any case.] (a) Variation in tangential velocity u_m/U_T at the most downstream control point of an impeller blade; (b) Variation in pressure difference $\Delta p_n/\rho_0 U_T^2$ at the same location.

Appendix A. Influence coefficients for the source panels

The influence coefficient vector $\mathbf{s}_j = (s_{1j}, s_{2j})$ will be given in terms of local coordinates for the jth panel, $(y_1, y_2)_j$, where the control point is at $(0,0)$ and the left and right corner at $(-s,0)$ and $(s,0)$, respectively. In these coordinates,

$$\tilde{\mathbf{s}}_j = (\tilde{s}_{1j}, \tilde{s}_{2j}) = \int_{-s}^{s} \left(\frac{y_1 - \xi, y_2}{(y_1 - \xi)^2 + y_2^2} \right)_j \mathrm{d}\xi$$
$$= \left(\frac{1}{2} \ln \left[\frac{(y_1 + s)^2 + y_2^2}{(y_1 - s)^2 + y_2^2} \right], \arctan\left(\frac{y_1 + s}{y_2} \right) - \arctan\left(\frac{y_1 - s}{y_2} \right) \right)_j . \tag{A.1}$$

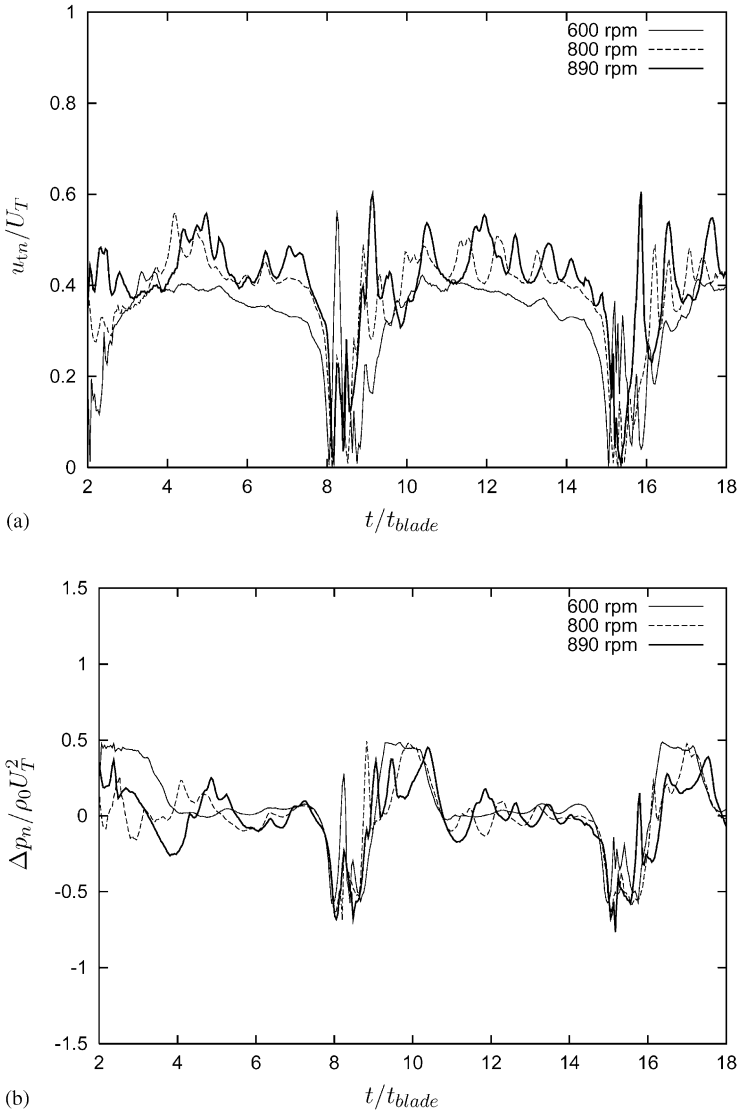

Fig. 13. Effect of pump speed. [The flow rate, in terms of inlet source strength, is kept constant.] (a) Variation in tangential velocity u_m/U_T at the most downstream control point of an impeller blade; (b) Variation in pressure difference $\Delta p_n/\rho_0 U_T^2$ at the same location.

Let $\mathbf{t}_j$ and $\mathbf{n}_j$ be the tangential and normal vector, respectively, to panel no. j, given in terms of global coordinates $\mathbf{X} = (X_1, X_2)$. The jth influence coefficient vector, given in these coordinates, is then

$$\mathbf{s}_j = \tilde{s}_{1j}\mathbf{t}_j + \tilde{s}_{2j}\mathbf{n}_j. \tag{A.2}$$

Let the control point of the jth panel be given by $\mathbf{y}_j$ in terms of global coordinates. For the case where the point of observation $\mathbf{x} = \mathbf{y}_j$, Eq. (A1) gives that

$$\tilde{s}_{1j} = 0, \quad \tilde{s}_{2j} = \pi. \tag{A.3}$$

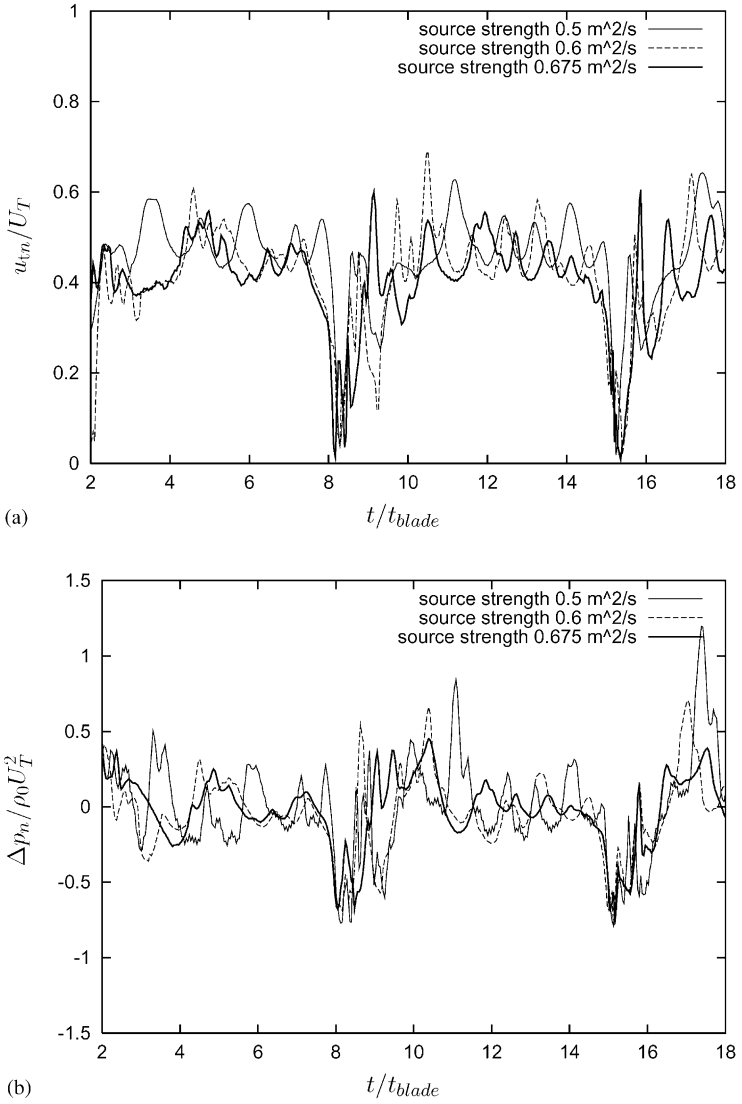

Fig. 14. Effect of flow rate, in terms of inlet source strength. [The pump speed is kept constant.] (a) Variation in tangential velocity u_{tn}/U_T at the most downstream control point of an impeller blade; (b) Variation in pressure difference $\Delta p_n/\rho_0 U_T^2$ at the same location.

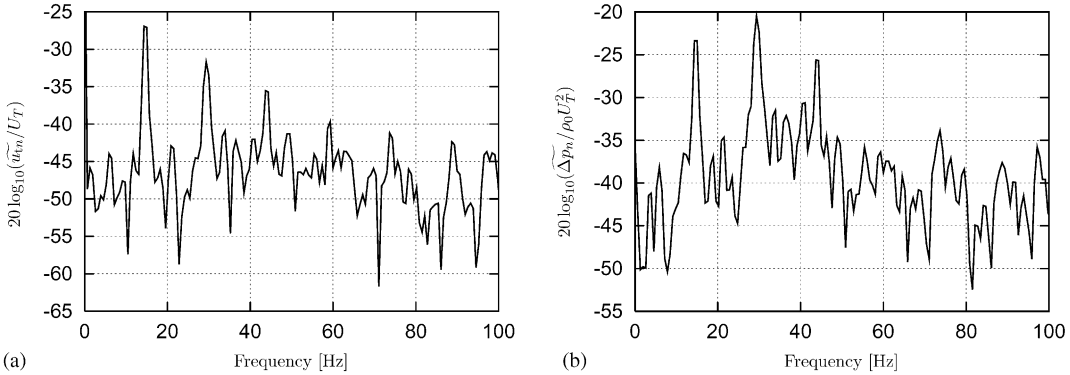

Fig. 15. (a) Frequency spectrum of the tangential velocity u_{tn}/U_T shown in Fig. 8(a) [Here $\tilde{\circ}$ denotes the Fourier transform of $\circ$.]; (b) Frequency spectrum of the tangential velocity pressure difference $\Delta p_n/\rho_0 U_T^2$ shown in Fig. 8(b).

References

Batchelor, G.K., 1967. An Introduction to Fluid Dynamics. Cambridge University Press, Cambridge.

Böhm, W., Farin, G., Kahmann, J., 1984. A survey of curve and surface methods in CAGD. Computer Aided Geometric Design 1, 1–60.

Brennen, C.E., 1994. Hydrodynamics of Pumps. Oxford University Press, Oxford.

Chu, S., Dong, R., Katz, J., 1995. Relationship between unsteady flow, pressure fluctuations, and noise in a centrifugal pump—Parts A and B. ASME Journal of Fluids Engineering 117, 24–35.

Cottet, G.-H., Koumoutsakos, P.D., 2000. Vortex Methods: Theory and Practice. Cambridge University Press, Cambridge.

Crighton, D.G., 1981. Acoustics as a branch of fluid mechanics. Journal of Fluid Mechanics 106, 261–298.

Crighton, D.G., 1985. The Kutta condition in unsteady flow. Annual Review of Fluid Mechanics 17, 411–445.

Cumpsty, N.A., 1977. A critical review of turbomachinery noise. ASME Journal of Fluids Engineering 99, 278–293.

Dong, R., Chu, S., Katz, J., 1997. Effect of modification to tongue and impeller geometry on unsteady flow, pressure fluctuations, and noise in a centrifugal pump. ASME Journal of Fluids Engineering 119, 506–515.

Drazin, P.G., Reid, W.H., 1981. Hydrodynamic Stability. Cambridge University Press, Cambridge.

Fedorchenko, A.T., 2000. On some fundamental flaws in present aeroacoustic theory. Journal of Sound and Vibration 232, 719–782.

Graham, J.M.R., 1986. Application of discrete vortex methods to the computation of separated flows. In: Morton, K.W., Baines, M.J. (Eds.), Numerical Methods for Fluid Dynamics II. Clarendon Press, Oxford, pp. 273–302.

Guelich, J.F., Bolleter, U., 1992. Pressure pulsations in centrifugal pumps. ASME Journal of Vibration and Acoustics 114, 272–279.

Howe, M.S., 1997. Sound generated by fluid–structure interactions. Computers & Structures 65, 433–446.

Howe, M.S., 1998. Acoustics of Fluid–Structure Interaction. Cambridge University Press, Cambridge.

Jeon, W.-H., Lee, D.J., 1999. An analysis of the flow and aerodynamic acoustic sources of a centrifugal impeller. Journal of Sound and Vibration 222, 505–511.

Jeon, W.-H., Lee, D.J., 2000. An analysis of generation and radiation of sound for a centrifugal fan. In: Proceedings of the Seventh International Congress of Sound and Vibration 2000, Garmisch-Partenkirchen, pp. 1235–1242.

Katz, J., Plotkin, A., 2001. Low-Speed Aerodynamics, 2nd Edition. Cambridge University Press, Cambridge.

Kiya, M., Sasaki, K., Arie, M., 1982. Discrete-vortex simulation of a turbulent separation bubble. Journal of Fluid Mechanics 120, 219–244.

Kuwahara, K., Takami, H., 1973. Numerical study of two-dimensional vortex motion by a system of point vortices. Journal of the Physical Society of Japan 9, 784–790.

Lanczos, C., 1956. Applied Analysis. Prentice-Hall, Englewood Cliffs, NJ (Reprinted 1988 by Dower, New York).

Langthjem, M.A., Olhoff, N., 2004. A numerical study of flow-induced noise in a centrifugal pump. Part II. Hydroacoustics. Journal of Fluids and Structures. This issue, doi:10.1016/j.jfluidstructs.2004.01.002

Lighthill, M.J., 1952. On sound generated aerodynamically. I. General theory. Proceedings of the Royal Society A 211, 564–587.

Lighthill, J., 1986. An Informal Introduction to Theoretical Fluid Mechanics. Oxford University Press, Oxford.

Mongeau, L., Thompson, D.E., McLaughlin, D.K., 1995. A method for characterizing aerodynamic sound sources in turbomachines. Journal of Sound and Vibration 181, 369–389.

Morgenroth, M., Weaver, D.S., 1996. Sound generation by a centrifugal pump at blade passage frequency. In: Proceedings of Flow-Induced Vibrations 1996, Montreal, pp. 455–463.

Neise, W., 1976. Noise reduction in centrifugal fans: a literature survey. Journal of Sound and Vibration 45, 375–403.

Qu, R., 1996. A new approach to numerical differentiation and integration. Mathematical and Computer Modelling 24, 55–68.

Rosenhead, L., 1931. The formation of vortices from a surface of discontinuity. Proceedings of the Royal Society of London A 134, 170–192.

Rzentkowski, G., 1996. Generation and control of pressure pulsations emitted from centrifugal pumps: a review. In: Proceedings of Flow-Induced Vibrations 1996, Montreal, pp. 439–454.

Rzentkowski, G., Zbroja, S., 2000. Experimental characterization of centrifugal pumps as an acoustic source at the blade-passing frequency. Journal of Fluids and Structures 14, 529–558.

Sarpkaya, T., 1988. Computational methods with vortices—the 1988 Freeman Scholar Lecture. ASME Journal of Fluids Engineering 111, 5–52.

Sarpkaya, T., Ihrig, C.J., 1986. Impulsively started steady flow about rectangular prisms: experiments and discrete vortex analysis. ASME Journal of Fluids Engineering 108, 47–54.

Satofuka, N. (Ed.), 2000. Computational Fluid Dynamics 2000. Springer, Berlin.

Stepanoff, A.J., 1957. Centrifugal and Axial Flow Pumps. Wiley, New York.

Sugimoto, N., Ogawa, T., 1998. Acoustic analysis of the pressure field in a tunnel, generated by entry of a train. Proceedings of the Royal Society A 454, 2083–2112.

Tryggvason, G., Dahm, W.J.A., Sbeih, K., 1991. Fine structure of vortex sheet rollup by viscous and inviscid simulation. ASME Journal of Fluids Engineering 113, 31–36.